

---

This is an electronic reprint of the original article.  
This reprint may differ from the original in pagination and typographic detail.

Monticeli, Francisco M.; Almeida Jr, Humberto; Neves, Roberta M.; Ornaghi Jr, Heitor;  
Trochu, François

**The influence of fabric architecture on impregnation behavior and void formation: Artificial neural network and statistical-based analysis**

*Published in:*  
Polymer Composites

*DOI:*  
[10.1002/pc.26578](https://doi.org/10.1002/pc.26578)

Published: 01/05/2022

*Document Version*  
Peer-reviewed accepted author manuscript, also known as Final accepted manuscript or Post-print

*Please cite the original version:*  
Monticeli, F. M., Almeida Jr, H., Neves, R. M., Ornaghi Jr, H., & Trochu, F. (2022). The influence of fabric architecture on impregnation behavior and void formation: Artificial neural network and statistical-based analysis. *Polymer Composites*, 43(5), 2812-2823. <https://doi.org/10.1002/pc.26578>

---

This material is protected by copyright and other intellectual property rights, and duplication or sale of all or part of any of the repository collections is not permitted, except that material may be duplicated by you for your research use or educational purposes in electronic or print form. You must obtain permission for any other use. Electronic or print copies may not be offered, whether for sale or otherwise to anyone who is not an authorised user.

# The influence of fabric architecture on impregnation behavior and void formation: ANN and statistical-based analysis

Francisco M. Monticeli<sup>1</sup>, José Humberto S. Almeida Jr.<sup>2,3\*</sup>, Roberta M. Neves<sup>4</sup>,  
Heitor L. Ornaghi Jr.<sup>5</sup>, François Trochu<sup>6</sup>

<sup>1</sup>Department of Materials and Technology, São Paulo State University, Guaratinguetá, SP, Brazil; [f.monticeli@unesp.br](mailto:f.monticeli@unesp.br)

<sup>2</sup>Department of Mechanical Engineering, Aalto University, Espoo, Finland; [humberto.almeida@aalto.fi](mailto:humberto.almeida@aalto.fi)

<sup>3</sup>Advanced Composites Research Group, School of Mechanical and Aerospace Engineering, Queen's University Belfast, UK

<sup>4</sup>PPGE3M, Federal University of Rio Grande do Sul, Porto Alegre, RS, Brazil; [robertamneves@gmail.com](mailto:robertamneves@gmail.com)

<sup>5</sup>Federal University for Latin American Integration (UNILA) Foz do Iguaçu, Paraná, Brazil; [ornaghijr.heitor@gmail.com](mailto:ornaghijr.heitor@gmail.com)

<sup>6</sup>Department of Mechanical Engineering, Research Center for High Performance Polymer and Composite Systems, Polytechnique Montréal, 2900 Boulevard Edouard Montpetit, Montréal, Québec H3T 1J4, Canada. [francois.trochu@polymtl.ca](mailto:francois.trochu@polymtl.ca)

\*Corresponding author. E-mail address: [humberto.almeida@aalto.fi](mailto:humberto.almeida@aalto.fi)

---

## Abstract

This work proposes an approach combining artificial neural networks (ANN) with statistical models to predict injection processing conditions for four reinforcement architectures: plain weave (PW), bidirectional non-crimp fabrics (NCF), unidirectional fabrics (Uni) and random fiber mats (Random). Key results allow evaluating the velocity of the flow front by combining processing parameters and creating a three-dimensional response surface based on a properly trained ANN. This investigation is based on a large number of experimental results. The key role played by some physical parameters was associated with predicting the impregnation behavior (velocity of the flow front) during resin injection. The main outcome aims to provide a better control of void content in terms of size and position to the four fibrous reinforcements considered.

**Keywords:** Permeability; RTM process; artificial neural network; void formation.

---

## 1. Introduction

Liquid composite molding (LCM) is a manufacturing technology with excellent cost benefits used to produce large and complex-shaped composite structures by resin injection or infusion.<sup>1-4</sup> Considering the continuous increase of polymer composite structural applications over the last decades,<sup>5</sup> understanding the physics of injection processing parameters and their complex relationships is essential to prevent the formation of defects such as porosity, warping, waviness, among others.<sup>6-8</sup> Indeed, controlling processing parameters **is critical in manufacturing** final parts of quality for structural applications with appropriate mechanical properties.<sup>9-11</sup> The resin transfer molding (RTM) process, for instance, depends on the fluid ability to percolate the reinforcement with appropriate viscosity. The reinforcement determines the resistance to the resin flow, which defines permeability<sup>12-14</sup> based on Darcy's law.<sup>15-17</sup>

The flow behavior can be used to control the formation and location of defects.<sup>18,19</sup> According to Patel et al.,<sup>20</sup> viscous drag forces among tows act at high flow front velocity, impregnating **the inter-tows regions firstly**, and hence increasing the creation of microscopic porosity inside tows. The opposite occurs at low flow velocity: capillary forces create a preferred impregnation inside tows, thus increasing the void content in the mesoporous network between fiber tows.<sup>21</sup> This phenomenon of void formation is caused by the physical interaction of the dual-scale fibrous reinforcement with the liquid resin.<sup>20,21</sup> Depending on the local velocity of the flow front, mesoscopic voids are usually found between fiber tows, while microscopic voids may appear inside tows.<sup>9,19,21</sup>

Two other factors that play a critical role in the impregnation behavior are the architecture of the fibrous material and the fiber volume fraction.<sup>22-24</sup> In addition, the various reinforcement architectures and different fiber volume fractions available for applications in structural composites can be processed with a wide range of injection parameters. This creates effective combinations of impregnation behaviors.<sup>25-28</sup> All these factors influence the impregnation flow and consequently the formation, morphology, and location of voids.<sup>25,27,29</sup> A complete analysis and classification are critical tasks to ensure high mechanical behavior since voids are connected to poor mechanical performance and the initiation of fracture mechanisms (crack initiation and propagation, delamination, tensile and shear strength, among others).<sup>30-32</sup> For instance, Hamidi et al.<sup>18</sup> emphasize the importance of characterizing void morphology, which can be even more detrimental to mechanical performance than void content.

Reports dealing with a reliability analysis<sup>33</sup> based on experiments aiming to enhance the impregnation behavior and quantify the contribution of each parameter to the flow front velocity and void formation presents a crucial subject to the scientific literature, mainly using mathematical approaches. Besides, this kind of experimental analysis can be time-consuming. Alternatively, an ANN could prove to be a more effective tool after training to analyze the impregnation of laminates compared to other statistical models.

This work proposes a methodology based on ANN and statistical analysis to investigate the role of injection parameters and material properties in impregnation behavior. In fact, as expected from experimental observations, the velocity of the flow front and the permeability of the fibrous reinforcement turn out to play key roles in that respect. For that purpose, the analysis of variance (ANOVA) and an analytical approach based on normal probability distributions will be applied here to evaluate the contributions of each processing parameter. An ANN is built and trained to predict the impregnation behavior and void formation (void content, morphology, and location) for each processing parameter (fiber volume fraction, architecture of the fibrous reinforcement, pressure, viscosity, and permeability). The ANN prediction data is then associated with the response surface methodology (RSM) to evaluate the permeability and the **front flow** velocity as a function of injection parameters. This statistical analysis confirms the key roles played by these physical parameters on the impregnation behavior and quality of high-performance composites fabricated by LCM.

## **2. Experimental investigations**

### **2.1. *Materials and processing parameters***

Aiming to provide a wide spectrum of data for the statistical models, data from a large number of published references on RTM and liquid resin infusion (LRI)<sup>12, 16, 17, 23, 26, 35–41, 43, 45–48, 50, 53, 54</sup> are aggregated for the statistical analysis as documented in the supplementary material. The kinds of reinforcements investigated are plain weave (PW) 1×1, a biaxial (0/90) non-crimp fabric (NCF), a unidirectional reinforcement (Uni), and a random fiber mat (Random). **All the reinforcing materials considered contain only glass fibers. The injection pressure lies in the range of 0.01 to 0.70 MPa. The viscosity varies between 50 and 520 mPa·s. The fiber volume fraction ( $V_f$ ) goes from 18 to 65%. To reduce calculations and simplify the prediction models, the linear flow front velocity is considered as a response in the ANN approach.**

## 2.2. Artificial neural network

Figure 1 shows the ANN consisting of input, output, and hidden layers. ANN is inspired by the central nervous system, in which each neuron represents processing elements that can perform operations such as calculations in parallel for data processing.<sup>55</sup>

Permeability is directly dependent of fiber volume fraction, and the other input parameters are independent parameters. However, the combination presents a correlation in the quality of the final composite, e.g., a high level of fiber volume fraction could require high pressure and low viscosity to ensure complete impregnation.

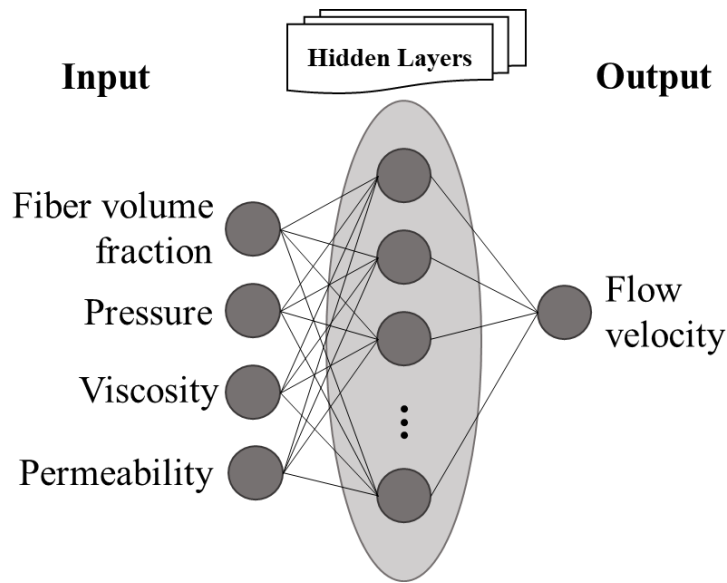


**Figure 1.** Schematic construction of an artificial neural network to correlate the two responses with the injection and material parameters on flow front velocity.

Figure 1 refers to the fiber volume fraction, pressure, viscosity, and permeability as input parameters and the front flow velocity as output. In fact, an activation function could describe a complex curve providing a more reliable data prediction. To calculate each prediction curve, an activation function needs to be applied to the input data to model the complex relationship between input variables and output terms. Appropriate activation functions allow fitting non-linear relationships between experimental data. The hyperbolic tangent is commonly used in multi-layer neural networks as a transfer function for complex experimental data distributions.<sup>56</sup>

$$f(x) = \frac{e^x - e^{-x}}{e^x + e^{-x}} \quad (1)$$

The activation function transforms the experimental data into a new dataset. For example, in the case of Equation 1, output values lie in the interval  $[-1,+1]$ . The goal is to reduce errors, aiming for a more precise prediction behavior. It is possible to generate a

prediction curve through repetition of calculations, thus finding an appropriate relationship between input parameters and output terms. Continuous recalculation of the activation function is a key factor here to improve the fitting accuracy. The weight algorithm was resilient backpropagation with **backtracking**, error function was the sum of squared errors, threshold of error function was 0.01. More precisions on the ANN procedure and definitions are given in the supplementary material, together with an example of application.

The dataset is used to adjust the connected nodes until the lower desired error level is reached. The error is characterized by the following  $B$  coefficient.<sup>57,58</sup>

$$B = 1 - \frac{\sum_{i=1}^n (Xp^{(i)} - X^{(i)})^2}{\sum_{i=1}^n (X^{(i)} - X)^2} \quad (2)$$

where  $Xp^{(i)}$  represents the predicted characteristic,  $X^{(i)}$  is the experimental value,  $X$  is the mean value of  $X^{(i)}$ , and  $n$  is the number of experimental data. The coefficient  $B$  describes how the output variable fits the experimental output data. It measures the fitting quality of the ANN output variable with the actual output test data. Higher  $B$  coefficients indicate that the ANN provides an improved approximation of output variables.

### 2.3. The statistical approach

The ANOVA methodology is also applied to perform variance analysis of the permeability and flow front velocity data to evaluate the contributions of fiber architecture, fiber volume fraction, pressure, and viscosity on the impregnation behavior. A single factor methodology is carried out to measure each parameter contribution to the responses. Parameters  $F_{critical}$  and  $p$ -value are calculated using the software MiniTab18,<sup>59</sup> which are standard from the Tables in Ref.<sup>60</sup> for  $\alpha = 5\%$ . **Table 1 describes how the factor  $F$  is calculated.**

**Table 1. The structured form of ANOVA.**

Variation	Sum of squares	Degrees of freedom	Square of means	$F$ factor
<b>Factor</b>	$S_a = \sum_{i=1}^c n(\bar{x}_i - \bar{\bar{x}})^2$	$V_a = C - 1$	$SM_a = \frac{S_a}{V_a}$	$F = \frac{SM_a}{SM_b}$
<b>Global</b>	$S_b = \sum_{i=1}^c \sum_{j=1}^n (x_{ji} - \bar{x}_i)^2$	$V_b = n - V_a$	$SM_b = \frac{S_b}{V_b}$	

where  $n$  is the number of experimental data,  $C$  is the number of groups (number of experimental data of each parameter),  $\bar{x}_i$  is the average of each group,  $\bar{x}$  represents the total average,  $x_{ji}$  is the  $F$  parameter representing the analysis factor to determine if the global parameter variation is greater than the variability of the observations within the analyzed parameter.

The normal distribution (frequency of data probability distribution) is also evaluated to estimate the permeability of each fabric architecture, the statistical distribution of flow front velocity, as well as the dispersion of these parameters.

The *Response Surface Methodology* (RSM – see Equation 3 below) analyzes the response trend using different levels of value for each parameter, which describes the interaction between the processing parameters on the permeability and flow front velocity.

$$Y = \beta_0 + \sum_{i=1}^k \beta_i x_i + \sum_{i=1}^k \beta_{ii} x_i^2 + \sum_{j=1}^k \beta_j x_j + \sum_{j=1}^k \beta_{jj} x_j^2 + \sum_{i=1}^{k-1} \sum_{j=i}^k \beta_{ji} x_i x_j \quad (3)$$

Where,  $Y$  represents the predicted response, i.e., the flow front velocity  $FV$  ( $\text{m}\cdot\text{s}^{-1}$ ),  $x_i$  and  $x_j$  are parameter values, where  $i$  represents the  $x$  axis (here the fiber volume fraction  $V_f$ ), and  $j$  the  $y$  axis (here the injection pressure  $P$ ). The parameter  $\beta_0$  is the constant coefficient,  $\beta_i$  the linear coefficients and  $\beta_{ij}$  is the interaction coefficients. This analysis is performed for each kind of fabric architecture considered.

### 3. Results and discussion

#### 3.1. Statistical analysis

Figure 2 shows the normal distributions of the linear flow front velocity. It is possible to notice a significant variation in both results for all the fibrous architectures explored in this investigation. Flow front velocity variations are expected since injection parameters such as pressure, viscosity, fiber volume fraction, and fiber architecture possess a large variability (see supplementary material for more information).

The normal distribution was calculated from the frequency of flow front velocity results for each kind of reinforcement. The results of Figure 2 indicate that the respective values the flow front velocity variation presents a different sequence: Uni > Random > PW > NCF, indicating a greater variation in velocity for specific combinations of process and material parameters. A similar trend was also reported in the scientific literature.<sup>12,23,25</sup>

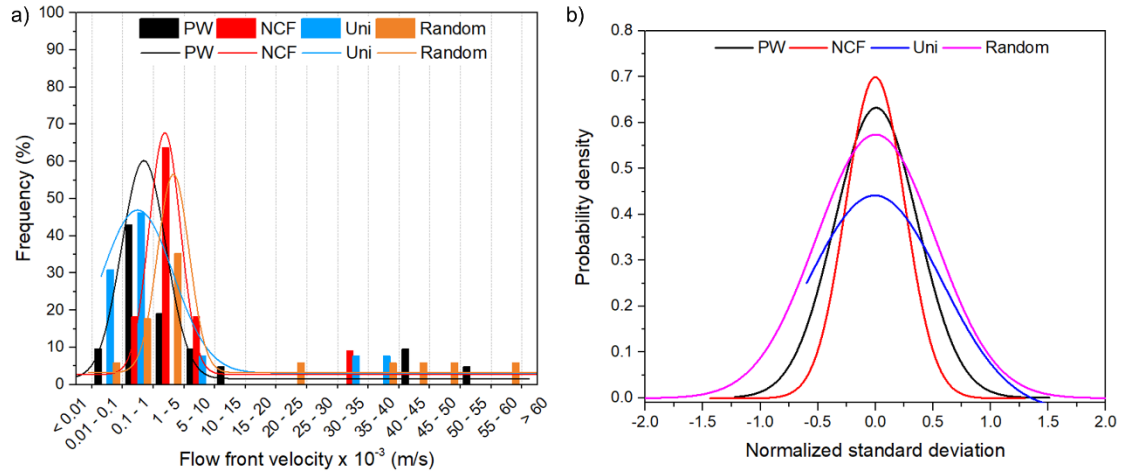


**Figure 2.** Histogram of impregnation data frequency for each kind of reinforcement: (a) flow front velocity and normal distributions, and (b) probability density vs. flow front velocity normalized fit ( $x$ -axis) derived from the histogram.

ANOVA was performed with  $\alpha = 0.05$  to provide 95% reliability. The null definition states that the population averages are all the same. In other words, the variations of one parameter do not affect the permeability and flow front velocity. The  $F_{critical}$  parameter is combined with the  $p$ -value in the analysis because a significant result does not mean that all variables play a critical role. The  $F_{critical}$  parameters define regions where test statistics are unlikely to lie. The  $p$ -values are the probability that test statistics be at least as extreme as the one observed, given that the null hypothesis is true or false.<sup>61</sup> The ANOVA definition is detailed in the supplementary material. The calculations of  $F_{critical}$  and  $p$ -values are also described in the supplementary material.

Table 2 lists the results of fiber volume fraction, pressure, and viscosity variance for permeability values reported for each fabric architecture to measure the influence of parameters on the impregnation behavior. The  $F_{critical}$  and  $p$ -value parameters are calculated using the software MiniTab18<sup>59</sup> as detailed in the supplementary material.  $F_{critical}$  is measured regarding the degree of freedom for all parameter combinations (for each reinforcement family).  $F$  values are calculated in Table 1.  $F_{critical}$  represents a limit value for the null hypothesis to hold, which indicates if one parameter **influences the response**.  $F$  is the calculated value of each parameter for all families of reinforcements studied, which describes each parameter variance compared with global variance. Finally, the  $p$ -value represents the probability of getting each  $F$  value.<sup>61</sup>

**Table 2.** ANOVA results for permeability

<b>PW</b>	<i>F</i>	<i>p-value</i>	<i>F<sub>critical</sub></i>
Fiber volume fraction	9.22	$3 \times 10^{-29}$	2.72
Pressure	0.27	$5 \times 10^{-6}$	2.72
Viscosity	0.45	$4 \times 10^{-8}$	2.72
<b>NCF</b>	<i>F</i>	<i>p-value</i>	<i>F<sub>critical</sub></i>
Fiber volume fraction	4.30	$4 \times 10^{-13}$	2.81
Pressure	0.43	$1 \times 10^{-6}$	2.81
Viscosity	0.25	$3 \times 10^{-5}$	2.81
<b>Uni</b>	<i>F</i>	<i>p-value</i>	<i>F<sub>critical</sub></i>
Fiber volume fraction	6.50	$3 \times 10^{-11}$	2.79
Pressure	0.32	$6 \times 10^{-6}$	2.79
Viscosity	0.12	$5 \times 10^{-11}$	2.79
<b>Random</b>	<i>F</i>	<i>p-value</i>	<i>F<sub>critical</sub></i>
Fiber volume fraction	8.23	$2 \times 10^{-10}$	2.74
Pressure	2.67	$4 \times 10^{-17}$	2.74
Viscosity	0.69	$2 \times 10^{-2}$	2.74

For PW fabric, the fiber volume fraction shows that  $F > F_{critical}$  with a  $p-value < 0.05$ . This means that the fiber volume fraction has an influence on the response. For pressure and viscosity,  $F < F_{critical}$  with  $p-value < 0.05$ . This indicates that both parameters (i.e., pressure and viscosity) are not reliable on a possible dependency of permeability.

NCF and Uni reinforcements exhibit the same behavior as PW, in which the fiber volume fraction is the main (and only) factor governing permeability since  $F > F_{critical}$  and  $p-value < 0.05$ . Pressure and viscosity are factors without influence on the response for both fiber architectures. In fact, permeability is independent of viscosity and pressure (at least in a first approximation based on the application of Darcy's law). Random mat also shows a similar behavior than previous reinforcements, with a higher  $F$  value for fiber volume fraction. The experimental results confirms that permeability is dependent on fiber volume fraction, and standard deviation presents no significant influence on response.

ANOVA demonstrated a low influence of pressure and viscosity on permeability, which depends only on the fiber volume fraction. This was expected because permeability characterizes the ability of the liquid to flow through the fiber bed. Nevertheless, this low

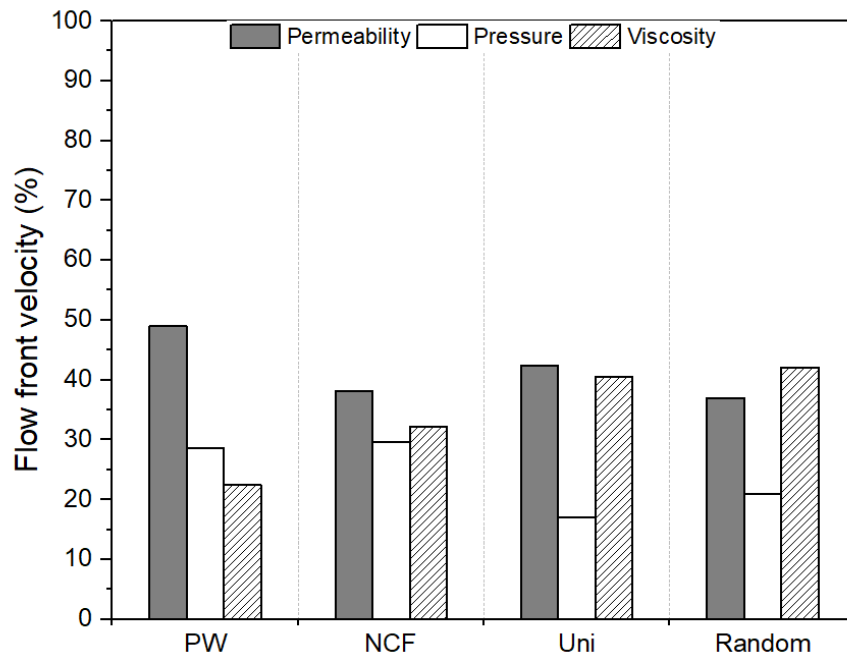
statistically observed contribution of pressure and viscosity may be associated with the variability of permeability measures. As a matter of fact, two benchmarks on in-plane permeability characterization have shown a significant dispersion in measured permeability data for the same procedure conditions.<sup>62</sup> This dispersion of experimental permeability results for the same fiber volume content induces a bias in the statistical response, leading to the values reported for the  $F$  and  $p$ -values. Therefore, a study considering the variability of manufacturing parameters becomes interesting, considering the reduction of results variance as a function of process parameters.

Table 3 lists the analysis of variance (ANOVA) for the flow front velocity. Since we know that the fiber volume fraction is intrinsically connected to permeability, confirmed by the previous statistical analysis, only permeability was considered as input together with pressure and viscosity in this analysis. All fiber architectures show that permeability governs the flow front velocity with  $F > F_{critical}$  and  $p$ -value  $< 0.05$ . Nevertheless, pressure and viscosity also exhibit  $F$  values higher than  $F_{critical}$ , presenting  $p$ -values  $< 0.05$ , which indicates that all parameters influence flow front velocity.

**Table 3.** ANOVA results for flow front velocity

<b>PW</b>	$F$	$p$ -value	$F_{critical}$
Permeability	8.52	$1 \times 10^{-28}$	2.72
Pressure	4.97	$5 \times 10^{-6}$	2.72
Viscosity	3.91	$2 \times 10^{-7}$	2.72
<b>NCF</b>	$F$	$p$ -value	$F_{critical}$
Permeability	5.51	$2 \times 10^{-7}$	2.81
Pressure	4.28	$1 \times 10^{-6}$	2.81
Viscosity	4.64	$4 \times 10^{-2}$	2.81
<b>Uni</b>	$F$	$p$ -value	$F_{critical}$
Permeability	12.91	$3 \times 10^{-11}$	2.79
Pressure	5.24	$6 \times 10^{-6}$	2.79
Viscosity	12.32	$6 \times 10^{-11}$	2.79
<b>Random</b>	$F$	$p$ -value	$F_{critical}$
Permeability	4.74	$8 \times 10^{-8}$	2.74
Pressure	2.67	$4 \times 10^{-17}$	2.74
Viscosity	5.39	$2 \times 10^{-2}$	2.74

Using ANOVA data, it is possible to calculate the percentage of contribution (PC) of each parameter to the flow front velocity. Figure 3 exhibits the PC for the flow front velocity, for which permeability is the main contributing factor (i.e., > 40%), followed by pressure and viscosity. Widely studied in the literature, all parameters present important contributions on the injection process; however, Figure 3 presents a comparative contribution analysis of each parameter, based on experimental analysis, in which several authors use constant viscosity associated with variation in fiber volume fraction and pressure levels, increasing their contribution to the response.



**Figure 3.** Percentage of contribution for flow front velocity.

The fiber volume fraction dictates the pressure required to ensure a complete impregnation of the fibrous reinforcement. Thus, this parameter is the main factor, and pressure is secondary. Fluid viscosity is also of utmost importance. However, there are limitations in resin viscosity. It is difficult to find an epoxy system of low viscosity (e.g., < 50 mPa.s) to ensure an appropriate impregnation time. Meanwhile, higher viscosity values might also make the impregnation unfeasible. Finally, a small range of viscosity values usually remains. In other words, the process limits the viscosity range levels, especially in studies that seek optimal injection approaches, focusing on lower viscosities to control the flow by other processes parameters. Thus, viscosity exhibits a lower influence on the response, to permit higher controllability of other parameters. <sup>63,64</sup>

### 3.2. Artificial neural network results

A dataset is constructed with injection parameters as input and impregnation behavior as output based on experimental data. The number of hidden neurons in each layer is twenty, and the optimal training data is twelve to ensure a reliable analysis with low error. The ANN results show an appropriate fit, in which the optimization parameters and validation are available in the supplementary material. Besides, the  $B$  coefficient introduced in Equation 2 is in accordance with the following sequence PW (0.95) > NCF and Uni (0.93) > Random (0.90). The Random preform shows the higher dispersion in prediction reliability ( $B$ -values = 0.85), because of high variations in experimental data. However, the  $B$ -values ensure a consistent prediction fit of the impregnation behavior.

Figures 4 and 5 show the experimental data and ANN predictions. The ANN predictions indicate that each processing and material parameter (fiber volume fraction, pressure, viscosity, and permeability) has an influence on the flow front velocity response. The fiber volume fraction acts directly as a restriction to the impregnation flow. However, this parameter provides mechanical properties such as stiffness and strength<sup>65</sup>. In the same way, viscosity is directly connected to the velocity of the flow front: a higher viscosity implies a greater difficulty of impregnation and a decreased flow front velocity. **On the other hand, the pressure parameter has** a direct influence on the flow path through fiber tows at low pressure or between tows at high pressure.<sup>20</sup>

Figure 4a shows the variations of fiber volume fraction against the flow front velocity. Both PW and NCF fabrics present a continuous decrease in flow front velocity **with all fiber volume fractions studied**. The Random preforms show an unusual variation on flow velocity decrease at 20% of fiber volume fraction, a plateau between 20 and 40%, and then the flow front velocity decreases more smoothly. The flow front velocity is lower for unidirectional reinforcements (Uni) than for PW, NCF, and Random reinforcements. However, Uni curve of flow front velocity demonstrates a continuous reduction for an increase in fiber volume fraction, but slightly away from the entire ANN prediction curve.

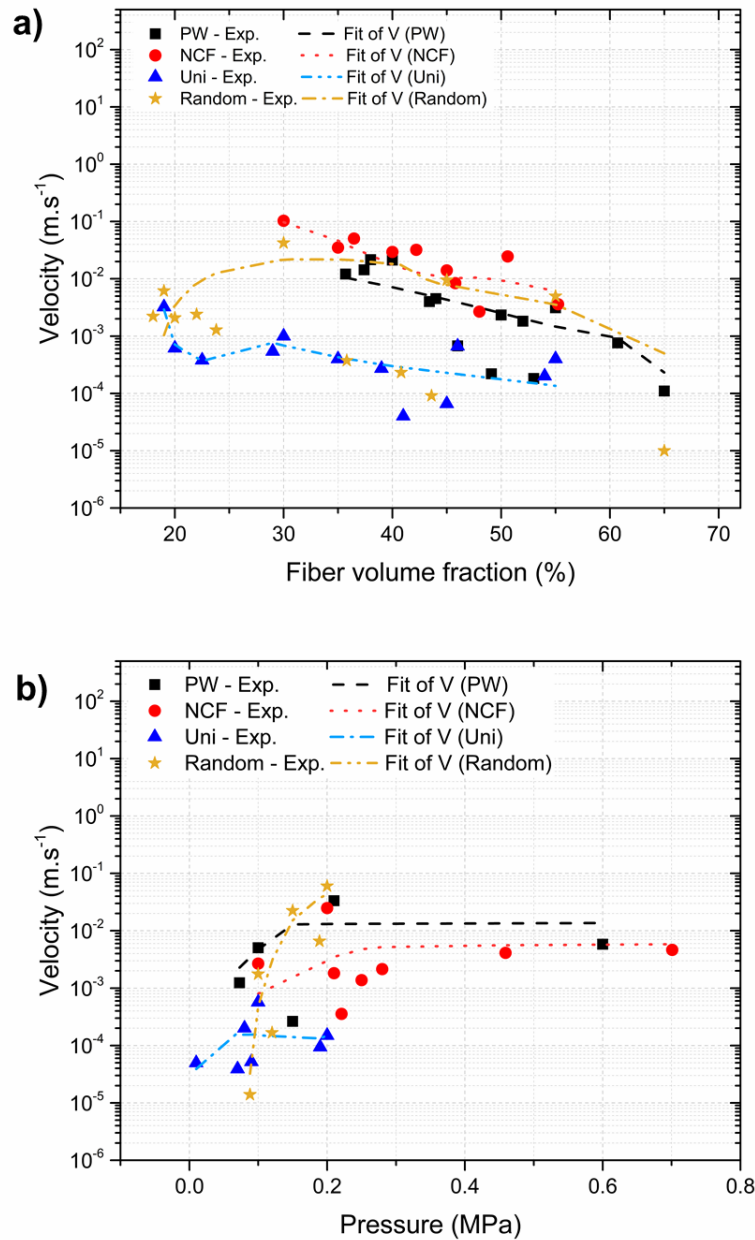


**Figure 4.** ANN flow front velocity predictions for each parameter: (a) fiber volume fraction; (b) pressure.

Figure 4b illustrates the ANN prediction of the flow front velocity as a function of pressure. The increase in pressure for the PW preform results in an abrupt increase of the flow front velocity up to a pressure of **0.22 MPa**, where a plateau with higher velocity occurs between **0.22** and **0.6 MPa**. The ANN prediction for **Random mats shows a significant increase in velocity up to a pressure of 0.2 MPa, indicating the correlation behavior between flow front velocity and pressure.** From that point, a plateau can be reached. For the NCF, the increase in pressure also generates an increase in velocity,

regarding the in-plane behavior in which the holes created by the sewing play a subordinate. NCF behaves like PW, but at a lower level.<sup>20</sup>

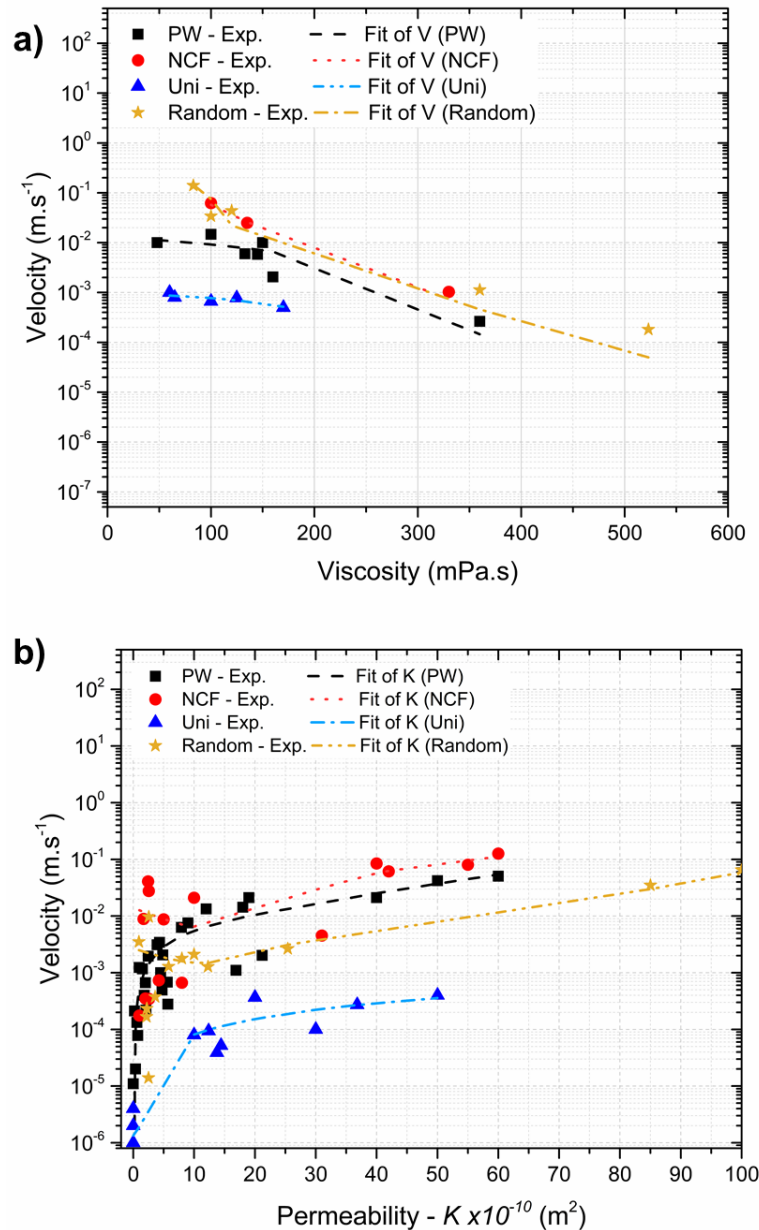


**Figure 5.** ANN flow front velocity predictions for each parameter: (a) viscosity; (b) permeability.

The viscosity variation (Figure 5a) shows that values greater than 200 mPa·s generate a significant decrease in the predicted velocity. It is difficult to maintain an appropriate impregnation flow to ensure low void formation with high viscosity matrix system for the injections process. Thus, it is suitable to control the flow front velocity by using larger injection parameters.<sup>66,67</sup> The NCF velocity shows the highest connection to permeability, followed by the PW, Random, and Uni. **The flow front velocity is directly proportional to permeability, but different slopes for each type of reinforcement.**

Figure 6 displays the architecture of each preform visually. The NCF (0/90) in Figure 6b has two preferential directions: the average flow direction can follow the orientations of the warp or of the weft of the fabric. This generates a balanced relationship with permeability and the impregnation flow front velocity. The PW (Figure 6a) has the same directions as the NCF fabric. However, the yarn weave increases tortuosity and the ability of the reinforcement layers to nest into each other,<sup>13,17</sup> thus decreasing permeability and hence the flow front velocity also. **Previous statements made for PW and NCF are only valid if both fabrics are balanced, i.e., the fiber content is the same in both directions. In addition, the fabric must have had the same warp and weft tension during manufacture and the weave type must also be symmetrical.**

The unidirectional arrangement (Figure 6c) exhibits a unique flow direction, which facilitates capillary flows, mainly at low velocity. The random reinforcement (Figure 6d) also presents a linear relationship between permeability and flow front velocity. However, the random architecture provides a higher slope than unidirectional fibers due to tortuosity.<sup>68</sup> In addition, random reinforcements exhibit a non-linear capillary effect and viscous drag force on the flow. **For the Uni and Random textiles, it should be noted that the capillary forces are usually one to two orders of magnitude smaller than the typical injection pressures and therefore do not usually play a role**

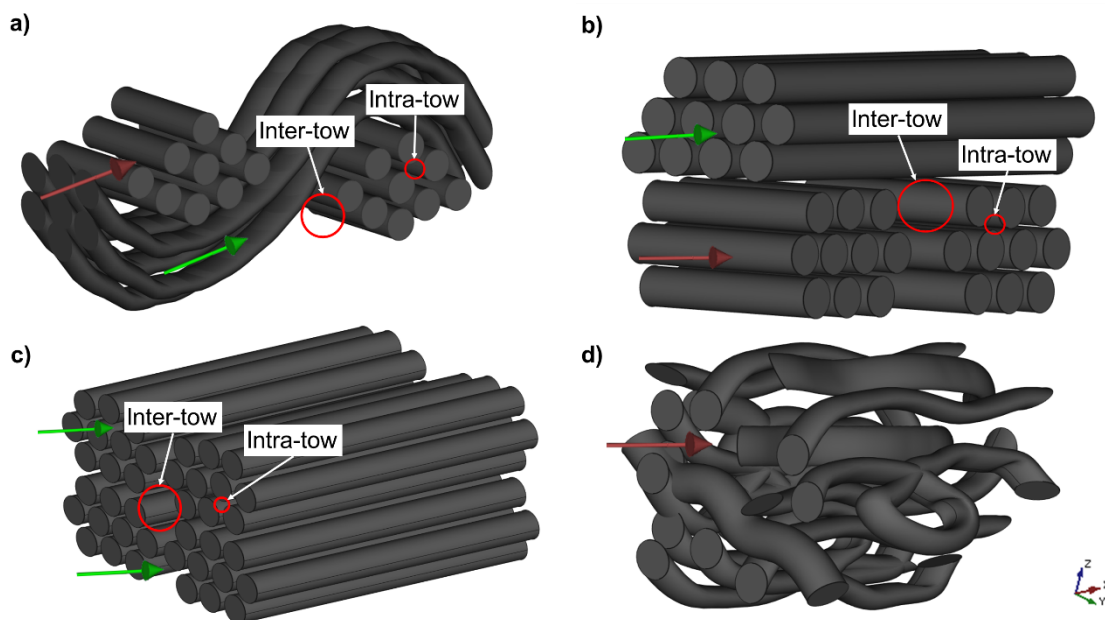


**Figure 6.** Schematic of fiber architectures: (a) PW; (b) NCF; (c) Uni; and (d) Random.

Ruiz et al.<sup>2,29</sup> and Patel et al.<sup>20</sup> presented an analytical model to predict void content and size based on the flow front velocity and a balance between capillary and viscous forces in the impregnation flow. Applying this restrictive model to the neural network, it

is also possible to predict void formation for each reinforcement architecture and assess the respective influence of both permeability and flow front velocity.

The velocity of the flow front is directly related to the formation, morphology and position of voids in terms of capillary and viscous drag effects. A low velocity creates capillary flow inside fiber tows, resulting in mesoscopic porosity between tows. Meanwhile, a higher flow front velocity creates a viscous drag, resulting in a faster flow between fiber tows and microscopic void formation inside tows.

As shown in Figure 7, the predicted results of void formation present a similar V shape as found in the scientific literature for the modified capillary number.<sup>2,29</sup> **The results of experimental porosity were extracted from experimental data and references, which also follows the equations  $V_{meso} = -32.3 - 11.8\log (FFV)$  and  $V_{micro} = 6.35 + 2.35\log (FFV)$ , which  $FFV$  is the flow front velocity.** The relationship between viscous and capillary effects can be confirmed for each fabric family analyzed. A mesoscopic void formation occurs for a flow front velocity lower than  $2 \times 10^{-3} \text{ m}\cdot\text{s}^{-1}$ , and microscopic voids appear for an average flow front velocity higher than  $2 \times 10^{-3} \text{ m}\cdot\text{s}^{-1}$ . Knowing this critical value of the flow front velocity, it is possible to control the void formation through resin injection. In addition, the determination of the injection parameters (pressure, viscosity, and fiber volume fraction) for each reinforcement family will be presented in *section 3.3*, in which the combination of the levels indicates the optimum impregnation flow front velocity.

Figure 8 shows, for all processing parameters, the void size-frequency predicted for each fibrous architecture – **calculated from Figure 7 data**. The PW and NCF fabrics display a higher trend of microscopic void formation ( $\approx 70\%$ ) since it is easier for the resin to flow between tows in **two main fabric directions**. Unidirectional flows create a greater capillary effect, which decreases the resistance to the impregnation flow at low velocity with a higher possibility of mesoscopic void creation between fiber tows. Random fiber mats present no differences in void size since random fiber mats are materials of single porosity, whereas all the other kinds of reinforcement **are considered** to possess a dual-scale porous structure.

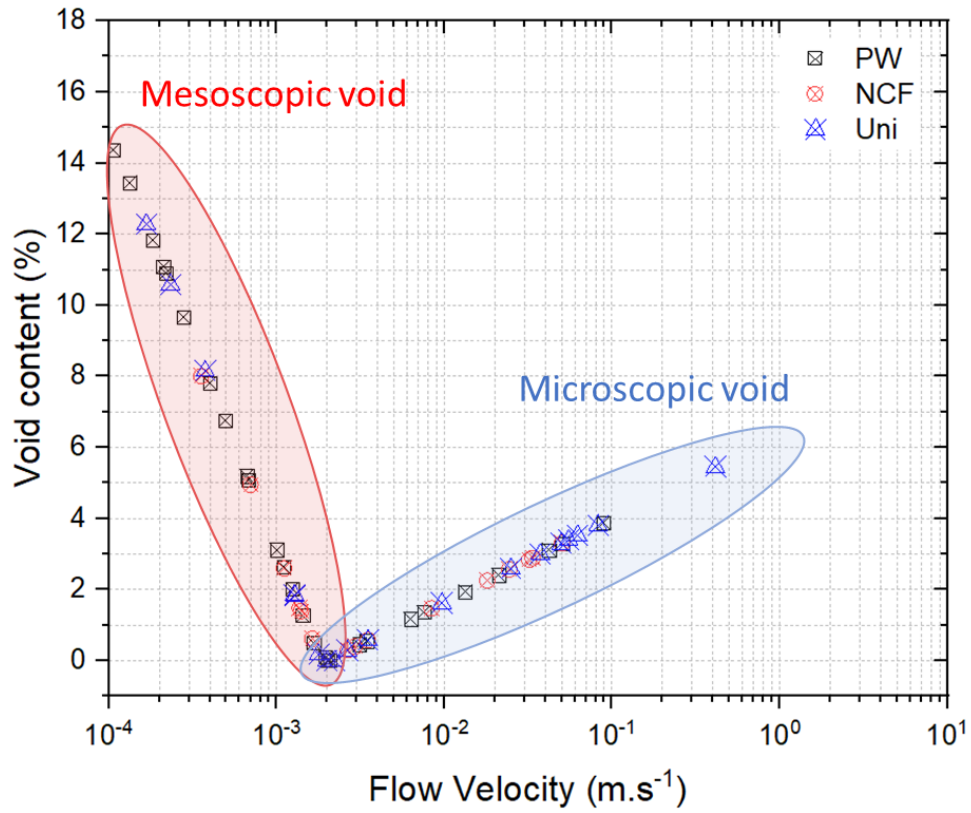


Figure 7. ANN Void content and morphology predictions flow front velocity.

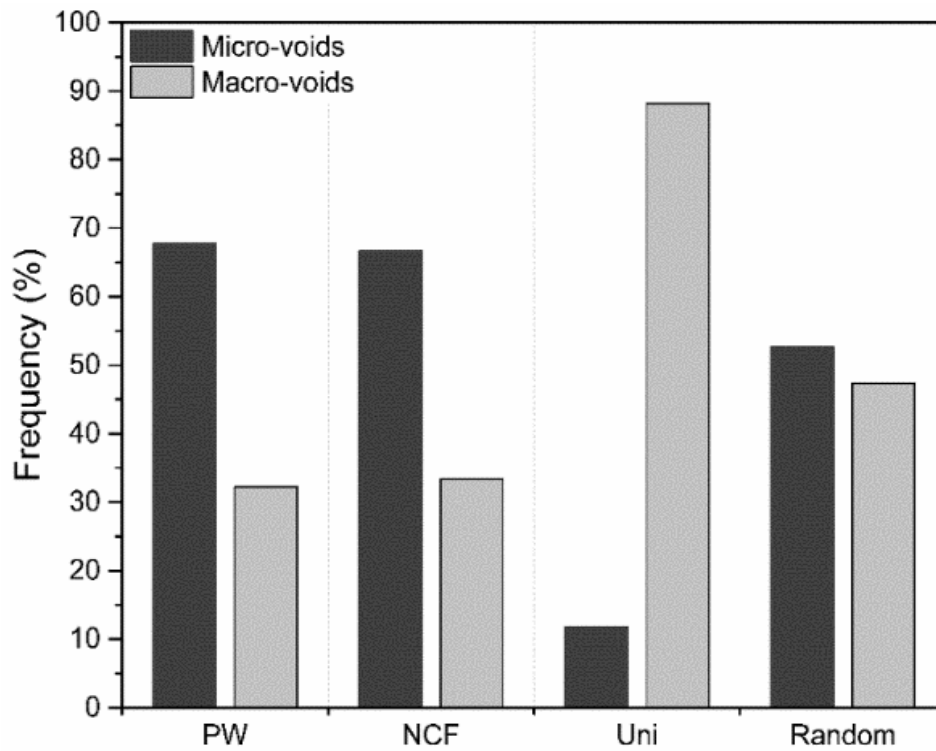


Figure 8. Microscopic and mesoscopic void content frequency.

### 3.3. Impregnation trends

This section presents a surface contour response in Figure 9 for the ANN prediction data to implement the RSM.<sup>69</sup> Each analysis provides an equation to predict the flow front velocity based on a combination of pressure and fiber volume fraction parameters, with a high-reliability level since the determining  $B$ -value  $> 0.9$  for all the reinforcements considered. All the response surfaces are calculated for a viscosity of 100 mPa·s because higher viscosity levels limit control of the flow as shown in the ANN prediction fit of Figure 4c. The dots are the ANN prediction data.

The SRM was performed based on Equation 3, through non-linear surface regression, in which the three-dimensional curve is obtained, with the variable response (flow front velocity) being plotted as a function of pressure vs. fiber volume fraction and constant viscosity. An example of the SRM development is described in the supplementary material. This analysis aims to model how changes in variables affect the flow front velocity, find the levels of variables that optimize the response, and select the operational conditions for void formation control. Based on the model generated by Figure 7, we can control the pore fraction and size based on the impregnation flow velocity. The statistical modeling of SRM provides the optimization of flow front velocity values, in which it is possible to determine the flow velocity following parameters combination and, as a consequence, determine the optimal void content/size. This explanation was added in the manuscript

Figure 9a exhibits the PW flow front velocity prediction surfaces of Equations (4). Both parameters (pressure and void volume fraction) contribute to the impregnation velocity. The use of low fiber fraction with low pressure results in higher flow velocity - associated with viscous drag force presence. On the other hand, the increase in fiber volume fraction results in a low flow front velocity, increasing the capillary effect. Based on the ideal flow front velocity given by the ANN analysis, a fiber volume fraction 55% associated with a pressure between 0.1 and 0.5 MPa represent optimal parameter levels to reduce void content and size.

Figure 9b depicts the NCF flow front velocity surfaces of Equations (5). The flow front velocity is also influenced by both parameters (fiber volume fraction and pressure). An appropriate flow front velocity to control void content and morphology lies in the range of 50 to 60 % for the fiber volume fraction associated with a pressure between 0.15 and 0.25 MPa.

Figure 9c exhibits flow front velocity surfaces for Uni reinforcements following Equations (6). Regarding the easier flow path in unidirectional preforms, which decreases the flow front velocity, a larger range of flow front velocity will reduce void formation, as shown in the central green region of Figure 9c. A broader range of optimal flow front velocity for Uni fibers is associated with chosen viscosity (100 mPa·s) since it allows a higher impregnation control. However, due to the direction of unidirectional reinforcements, a small modification of injection parameters could facilitate the effect of the viscous force (a combination of higher pressure and lower fiber volume content) or increase the capillary effect (lower pressure with higher fiber volume content).

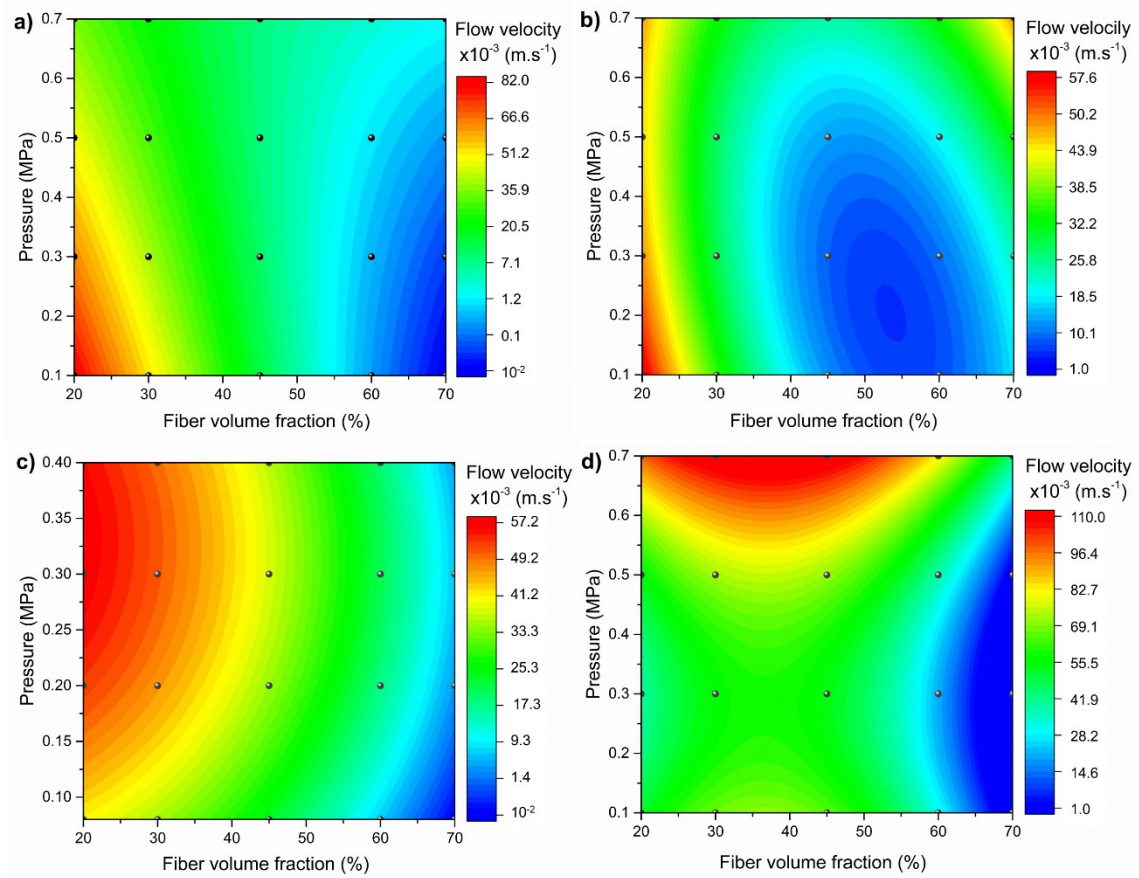


**Figure 9.** Response surface trend behavior as a function of pressure and fiber volume fraction flow front velocity: (a) PW, (b) NCF, (c) Uni, and (d) Random.

$$\text{Flow front velocity} = 176 - 3.9V_f - 162P + 0.01V_f^2 + 30P^2 + 2.8V_fP \quad (4)$$

$$\text{Flow front velocity} = 136 - 4.8V_f - 39P + 0.04V_f^2 - 22P^2 + 1.2V_fP \quad (5)$$

$$\text{Flow front velocity} = 1.6 - 0.002V_f + 23P + 0.001V_f^2 - 34P^2 - 0.03V_fP \quad (6)$$

$$\text{Flow front velocity} = 0.1 + 5V_f - 197P - 0.07V_f^2 + 339P^2 + 0.2V_fP \quad (7)$$

Figure 9d shows the flow front velocity surfaces of Random reinforcements associated with Equations (7). The flow front velocity is influenced by both parameters (fiber volume fraction and pressure) and presents similar trends. The optimal flow front velocity to control void content and morphology is not directly predicted since the random fiber directions do not allow control of viscous drag forces and capillary effects. However, the current method uses the results of the flow front velocity trend to control the impregnation behavior in random fiber mats.

#### 4. Conclusions

This study evaluated the role of injection parameters on the impregnation behavior and void formation in composite laminates by a statistical approach and ANN methodology. Three fiber architectures and random fiber mats were analyzed. For PW, NCF, and Uni reinforcements, the ANOVA analysis confirmed that the fiber volume fraction is the factor used to determine the permeability. For the flow front velocity, all parameters influence the injection process; however, with a distinct comparative contribution for each parameter. Random fiber mats showed dispersion in the response, which resulted in the lower reliable analysis regarding the variation for each mat. The combination of the statistical and ANN methods allows predicting the flow front velocity by combining injection process parameters for all the fiber architectures used in this study, making it possible to choose appropriate parameters to ensure proper control of void content and position as a function of processing levels combinations not accessed experimentally.

#### Acknowledgments

The authors acknowledge the financial support from FAPESP [Grant No. 2017/10606-4] and CAPES [Financial code 001]. JHS Almeida Jr thanks the Royal Academy of Engineering under the Research Fellowship scheme [Grant No. RF/201920/19/150].

#### References

1. Li M, Wang SK, Gu YZ, Li YX, Potter K, Zhang ZG. Evaluation of through-thickness permeability and the capillary effect in vacuum assisted liquid molding process. *Compos Sci Technol* 2012;72:873–8. <https://doi.org/10.1016/j.compscitech.2012.02.014>.

2. Ruiz E, Achim V, Soukane S. Advanced numerical simulation of liquid composite molding for process analysis and optimization *Franc. Compos Part A Appl Sci Manuf* 2006;37:890–902. <https://doi.org/10.1016/j.compositesa.2005.06.003>.
3. Lawrence JM, Neacsu V, Advani SG. Modeling the impact of capillary pressure and air entrapment on fiber tow saturation during resin infusion in LCM. *Compos Part A Appl Sci Manuf* 2009;40:1053–64. <https://doi.org/10.1016/j.compositesa.2009.04.013>.
4. Heider D, Simacek P, Dominauskas A, Deffor H, Advani S, Gillespie JW. Infusion design methodology for thick-section, low-permeability preforms using inter-laminar flow media. *Compos Part A Appl Sci Manuf* 2007;38:525–34. <https://doi.org/10.1016/j.compositesa.2006.02.016>.
5. Roberts T. The Carbon Fibre Industry: Global Strategic Market Evaluation 2011-2020. *Mater Technol Publ* 2011:1–12.
6. Uhlig K, Bittrich L, Spickenheuer A, Almeida Jr. JHS. Waviness and fiber volume content analysis in continuous carbon fiber reinforced plastics made by tailored fiber placement. *Compos Struct* 2019;222. <https://doi.org/10.1016/j.compstruct.2019.110910>.
7. Tuncol G, Danisman M, Kaynar A, Sozer EM. Constraints on monitoring resin flow in the resin transfer molding (RTM) process by using thermocouple sensors. *Compos Part A Appl Sci Manuf* 2007;38:1363–86. <https://doi.org/10.1016/j.compositesa.2006.10.009>.
8. Ferland P, Guittard D, Trochu F. Concurrent Methods for Permeability Measurement in Resin Transfer Molding. *Polym Compos* 1996;17:149–58. <https://doi.org/10.3139/9781569906200.016>.
9. Bodaghi M, Cristóvão C, Gomes R, Correia NC. Experimental characterization of voids in high fibre volume fraction composites processed by high injection pressure RTM. *Compos Part A* 2016;82:88–99.
10. Hamidi YK, Aktas L, Altan MC. Effect of packing on void morphology in resin transfer molded E-glass/ epoxy composites. *Polym Compos* 2005;26:614–27. <https://doi.org/10.1002/pc.20132>.
11. Hamidi YK, Altan MC. Process Induced Defects in Resin Transfer Moulding. *Int Polym Process* 2017;32:527–44.
12. Luo Y, Verpoest I, Hoes K, Vanheule M, Sol H, Cardon A. Permeability measurement of textile reinforcements with several test fluids. *Compos - Part A Appl Sci Manuf* 2001;32:1497–504. [https://doi.org/10.1016/S1359-835X\(01\)00049-5](https://doi.org/10.1016/S1359-835X(01)00049-5).
13. da Silva AAX, Souza JA, Manes A, Amico SC. In-plane Permeability and Mechanical Properties of R-Glass / Aramid Hybrid Composites. *J Mater Eng Perform* 2020:1–9. <https://doi.org/10.1007/s11665-020-04944-1>.
14. Chatel S, Maison-le-Poec S, Trochu F, Ruiz E, Bréard J, Ouagne P. A Permeability Measurement Method Dedicated to a Composite Process Family. *9th Int Conf Flow Porc Compos* 2008;9:8–10.
15. Chan AW, Larive DE, Morgan RJ. Anisotropic Permeability of Fiber Preforms: Constant Flow Rate Measurement. *J Compos Mater* 1993;27:996–1008. <https://doi.org/10.1177/002199839302701003>.
16. Härter FV, Souza JA, Isoldi LA, Santos ED Dos, Amico SC. Transverse permeability determination and influence in resin flow through an orthotropic medium in the RTM process. *Rev Mater* 2017;22. <https://doi.org/10.1590/s1517-707620170002.0167>.
17. Monticeli FM, Silva Monte Vidal DC, Shiino MY, Voorwald HJC, Cioffi MOH. Hybrid-permeability model evaluation through concepts of tortuosity and resistance rate: Properties of manufactured hybrid laminate. *Polym Eng Sci* 2019;59:1215–22. <https://doi.org/10.1002/pen.25104>.
18. Hamidi YK, Aktas L, Altan MC. Three-dimensional features of void morphology in resin transfer molded composites. *Compos Sci Technol* 2005;65:1306–20. <https://doi.org/10.1016/j.compscitech.2005.01.001>.
19. Etemadi R, Pillai K, Rohatgi P, Hamidi SA. On Porosity Formation in Metal Matrix Composites Made with Dual-Scale Fiber Reinforcements Using Pressure Infiltration Process. *Metall Mater Trans A* 2015;46:2119–33. <https://doi.org/10.1007/s11661-015-2792-9>.

20. Patel N, Rohatgi V, Lee LJ. Micro scale flow behavior and void formation mechanism during impregnation through a unidirectional stitched fiberglass mat. *Polym Eng Sci* 1995;35:837–51. <https://doi.org/10.1002/pen.760351006>.
21. Causse P, Ravey C, Trochu F. Capillary Characterization of Fibrous Reinforcement and Optimization of Injection Strategy in Resin Transfer Molding. *J Compos Sci* 2018;2:19. <https://doi.org/10.3390/jcs2020019>.
22. Lam RC, Kardos JL. The permeability and compressibility of aligned and cross-ply carbon fiber beds during processing of composites. *Polym Eng Sci* 1991;31:1064–70. <https://doi.org/10.1002/pen.760311411>.
23. Binétruy C, Pabiot J. Effects of fabric architectural heterogeneities on effective and saturated permeabilities in RTM. *Proc ICCM12, Paris* 1999:5–7.
24. Demaría C, Ruiz E, Trochu F. In-Plane Anisotropic Permeability Characterization of Deformed Woven Fabrics by Unidirectional Injection. Part II: Prediction Model and Numerical Simulations. *Polym Compos* 2007;28:812–27. <https://doi.org/10.1002/pc>.
25. Salvatori D, Caglar B, Teixidó H, Michaud V. Permeability and capillary effects in a channel-wise non-crimp fabric. *Compos Part A Appl Sci Manuf* 2018;108:41–52.
26. Di Fratta C, Klunker F, Ermanni P. Characterization of textile permeability as a function of fiber volume content with a single unidirectional injection experiment. *Compos Part A Appl Sci Manuf* 2015;77:238–47.
27. Galpayage Dona KNU, Du E, Carlsson LA, Fletcher DMK, Boardman RP. Modeling of water wicking along fiber/matrix interface voids in unidirectional carbon/vinyl ester composites. *Microfluid Nanofluidics* 2020;24:31:1-9. <https://doi.org/10.1007/s10404-020-02332-8>.
28. Rimmel O, May D. Modeling transverse micro flow in dry fiber placement preforms. *J Compos Mater* 2020;54:1691–703. <https://doi.org/10.1177/0021998319884612>.
29. Ruiz E, Achim V, Soukane S, Trochu F, Bréard J. Optimization of injection flow rate to minimize micro/macro-voids formation in resin transfer molded composites. *Compos Sci Technol* 2006;66:475–86. <https://doi.org/10.1016/j.compscitech.2005.06.013>.
30. Zhang Y, Zhang L, Yin X, Liu Y, He Z, Zhang J. Effects of porosity on in-plane and interlaminar shear strengths of two-dimensional carbon fiber reinforced silicon carbide composites. *Mater Des* 2016;98:120–7. <https://doi.org/10.1016/j.matdes.2016.03.017>.
31. Li Y, Li Q, Ma H. The voids formation mechanisms and their effects on the mechanical properties of flax fiber reinforced epoxy composites. *Compos PART A* 2015;72:40–8. <https://doi.org/10.1016/j.compositesa.2015.01.029>.
32. Almeida M De, Cerqueira M, Leali M. The influence of porosity on the interlaminar shear strength of carbon / epoxy and carbon / bismaleimide fabric laminates. *Compos Sci Technol* 2001;61:2101–8.
33. Wang Z, S. Almeida Jr. JH, St-Pierre L, Wang Z, P. Castro SG. Reliability-based buckling optimization with an accelerated Kriging metamodel for filament-wound variable angle tow composite cylinders. *Compos Struct* 2020:112821. <https://doi.org/https://doi.org/10.1016/j.compstruct.2020.112821>.
34. Barkoula NM, Alcock B, Cabrera NO, Peijs T. Flame-Retardancy Properties of Intumescent Ammonium Poly(Phosphate) and Mineral Filler Magnesium Hydroxide in Combination with Graphene. *Polym Polym Compos* 2008;16:101–13. <https://doi.org/10.1002/pc>.
35. Oliveira IR, Amico SC, Souza JA, Barbosa De Lima AG. Numerical analysis of the resin transfer molding process via PAM-RTM software. *Defect Diffus Forum* 2015;365:88–93. <https://doi.org/10.4028/www.scientific.net/DDF.365.88>.
36. Ma Y, Shishoo R. Permeability characterization of different architectural fabrics. *J Journal Compos Mater* 1999;33:729–50.
37. Gebart BR. Permeability of Unidirectional Reinforcements for RTM. *J Compos Mater* 1992;26:1100–33. <https://doi.org/10.1177/002199839202600802>.
38. Gauvin R, Kerachni A, Fisa B. Variation of mat surface density and its effect on permeability evaluation for RTM modelling. *J Reinf Plast Compos* 1994;13:371–83. <https://doi.org/10.1177/073168449401300408>.

39. Schmidt TM, Goss TM, Amico SC, Lekakou C. Permeability of hybrid reinforcements and mechanical properties of their composites molded by resin transfer molding. *J Reinf Plast Compos* 2009;28:2839–50. <https://doi.org/10.1177/0731684408093974>.
40. Rodríguez E, Giacomelli F, Vazquez A. Permeability-porosity relationship in RTM for different fiberglass and natural reinforcements. *J Compos Mater* 2004;38:259–68. <https://doi.org/10.1177/0021998304039269>.
41. Amico S, Lekakou C. An experimental study of the permeability and capillary pressure in resin-transfer moulding. *Compos Sci Technol* 2001;61:1945–59. [https://doi.org/10.1016/S0266-3538\(01\)00104-X](https://doi.org/10.1016/S0266-3538(01)00104-X).
42. Steenkamer DA, McKnight SH, Wilkins DJ, Karbhari VM. Experimental characterization of permeability and fibre wetting for liquid moulding. *J Mater Sci* 1995;30:3207–15. <https://doi.org/10.1007/BF01209239>.
43. Lekakou C, Johari MAK, Norman D, Bader MG. Measurement techniques and effects on in-plane permeability of woven cloths in resin transfer moulding. *Compos Part A Appl Sci Manuf* 1996;27:401–8. [https://doi.org/10.1016/1359-835X\(95\)00028-Z](https://doi.org/10.1016/1359-835X(95)00028-Z).
44. Nedanov PB, Advani SG. A Method to Determine 3D permeability. *J Compos Mater* 2002;36:241–54. <https://doi.org/10.1106/002199802021462>.
45. Zhang F, Cosson B, Comas-Cardona S, Binetruy C. Efficient stochastic simulation approach for RTM process with random fibrous permeability. *Compos Sci Technol* 2011;71:1478–85. <https://doi.org/10.1016/j.compscitech.2011.06.006>.
46. Saouab A, Bréard J, Lory P, Gardarein B, Bouquet G. Injection simulations of thick composite parts manufactured by the RTM process. *Compos Sci Technol* 2001;61:445–51. [https://doi.org/10.1016/S0266-3538\(00\)00126-3](https://doi.org/10.1016/S0266-3538(00)00126-3).
47. Han KK, Lee CW, Rice BP. Measurements of the permeability of fiber preforms and applications. *Compos Sci Technol* 2000;60:2435–41. [https://doi.org/10.1016/S0266-3538\(00\)00037-3](https://doi.org/10.1016/S0266-3538(00)00037-3).
48. Salvatori D, Caglar B, Teixidó H, Michaud V. Permeability and capillary effects in a channel-wise non-crimp fabric. *Compos Part A Appl Sci Manuf* 2018;108:41–52. <https://doi.org/10.1016/j.compositesa.2018.02.015>.
49. Morren G, Bossuyt S, Sol H. 2D permeability tensor identification of fibrous reinforcements for RTM using an inverse method. *Compos Part A Appl Sci Manuf* 2008;39:1530–6. <https://doi.org/10.1016/j.compositesa.2008.05.019>.
50. Li J, Zhang C, Liang R, Wang B. Statistical characterization and robust design of RTM processes. *Compos Part A Appl Sci Manuf* 2005;36:564–80. <https://doi.org/10.1016/j.compositesa.2004.10.001>.
51. Hoes K, Dinescu D, Sol H, Parnas RS, Lomov S. Study of nesting induced scatter of permeability values in layered reinforcement fabrics. *Compos Part A Appl Sci Manuf* 2004;35:1407–18. <https://doi.org/10.1016/j.compositesa.2004.05.004>.
52. Hoes K, Dinescu D, Sol H, Vanheule M, Parnas RS, Luo Y, et al. New set-up for measurement of permeability properties of fibrous reinforcements for RTM. *Compos - Part A Appl Sci Manuf* 2002;33:959–69. [https://doi.org/10.1016/S1359-835X\(02\)00035-0](https://doi.org/10.1016/S1359-835X(02)00035-0).
53. Wei B-J, Chang Y-S, Yao Y, Fang J. Online Estimation and Monitoring of Local Permeability in Resin Transfer Molding. *Polym Compos* 2016;37:1249–58. <https://doi.org/10.1002/pc.23290>.
54. Cazaux G, Bizet L, Bréard J, Gomina M, Syerko E, Comas-Cardona S, et al. Permeability enhancement with different glass fiber quasi-UD structure arrangements for RTM-TP process. *ICCM Int Conf Compos Mater* 2015;2015-July.
55. Fernández-Fdz D, López-Puente J, Zaera R. Prediction of the behaviour of CFRPs against high-velocity impact of solids employing an artificial neural network methodology. *Compos Part A Appl Sci Manuf* 2008;39:989–96. <https://doi.org/10.1016/j.compositesa.2008.03.002>.
56. Paneiro G, Durão FO, Costa e Silva M, Falcão Neves P. Artificial neural network model for ground vibration amplitudes prediction due to light railway traffic in urban areas. *Neural Comput Appl* 2018;29:1045–57. <https://doi.org/10.1007/s00521-016-2625-9>.

57. Fausett L. *Fundamentals of Neural Networks: Architectures, Algorithms and Applications*. vol. 1st editio. 1994.
58. Zhang Z, Klein P, Friedrich K. Dynamic mechanical properties of PTFE based short carbon fibre reinforced composites: Experiment and artificial neural network prediction. *Compos Sci Technol* 2002;62:1001–9. [https://doi.org/10.1016/S0266-3538\(02\)00036-2](https://doi.org/10.1016/S0266-3538(02)00036-2).
59. ANOVA. ANOVA - MiniTab18. <https://SupportMinitabCom/Pt-Br/Minitab/18/Help-and-How-to/Modeling-Statistics/Anova/Supporting-Topics/Basics/What-Is-Anova/> 2021:2–3.
60. Montgomery DC. *Design and Analysis of Experiments*. 2017. <https://doi.org/10.1002/9783527809080.cataz11063>.
61. Asiltürk I, Neşeli S, Ince MA. Optimisation of parameters affecting surface roughness of Co28Cr6Mo medical material during CNC lathe machining by using the Taguchi and RSM methods. *Meas J Int Meas Confed* 2016;78:120–8. <https://doi.org/10.1016/j.measurement.2015.09.052>.
62. May, D. et al. In-plane permeability characterization of engineering textiles based on radial flow experiments: A benchmark exercise. *Composites Part A* 2019;121:100–114. <https://doi.org/10.1016/j.compositesa.2019.03.006>.
63. Garschke C, Weimer C, Parlevliet PP, Fox BL. Out-of-autoclave cure cycle study of a resin film infusion process using in situ process monitoring. *Compos Part A Appl Sci Manuf* 2012;43:935–44. <https://doi.org/10.1016/j.compositesa.2012.01.003>.
64. Vernet N, Ruiz E, Advani S, Alms JB, Aubert M, Barburski M, et al. Experimental determination of the permeability of engineering textiles : Benchmark II. *Compos - Part A Appl Sci Manuf* 2014;61:172–84. <https://doi.org/10.1016/j.compositesa.2014.02.010>.
65. Gu W, Wu HF, Kampe SL, Lu GQ. Volume fraction effects on interfacial adhesion strength of glass-fiber-reinforced polymer composites. *Mater Sci Eng A* 2000;277:237–43. [https://doi.org/10.1016/S0921-5093\(99\)00528-6](https://doi.org/10.1016/S0921-5093(99)00528-6).
66. Garschke C, Parlevliet PP, Weimer C, Fox BL. Cure kinetics and viscosity modelling of a high-performance epoxy resin film. *Polym Test* 2013;32:150–7. <https://doi.org/10.1016/j.polymertesting.2012.09.011>.
67. Zhang D, Wang R, Farhan S, Cai Y, Liu J. Chemorheological behaviors of TDE-85 toughened by low viscosity liquid epoxy for RTM process. *Polym Test* 2018;70:310–9. <https://doi.org/10.1016/j.polymertesting.2018.07.016>.
68. Otomo R, Mori K. Analysis of fluid permeability in tortuous fibrous bed based on pore radius distribution. *J Vis* 2020;23:71–80. <https://doi.org/10.1007/s12650-019-00613-1>.
69. Monticeli FM, Almeida JHS, Neves RM, Ornaghi FG, Ornaghi HL. On the 3D void formation of hybrid carbon/glass fiber composite laminates: A statistical approach. *Compos Part A Appl Sci Manuf* 2020;137:106036. <https://doi.org/10.1016/j.compositesa.2020.106036>.